UNDULATOR RADIATION IN A WAVEGUIDE

G. Geloni, E. Saldin, E. Schneidmiller and M. Yurkov
Deutsches Elektronen-Synchrotron (DESY), Hamburg, Germany

Abstract

We propose an analytical characterization of undulator radiation near resonance, when the presence of the vacuum-pipe affects radiation properties, as for the far-infrared undulator beamline at FLASH, that is designed to deliver pulses in the THz range. Such line can be used for pump-probe experiments where THz pulses are naturally synchronized to the VUV pulse from the FEL, as well as the development of novel electron-beam diagnostics techniques. Since the THz radiation diffraction-size exceeds the vacuum-chamber dimensions, characterization of infrared radiation must be performed accounting for the presence of a waveguide. We developed a theory of undulator radiation in a waveguide based on paraxial and resonance approximation. We solved the field equation with a tensor Green's function technique, and extracted figures of merit describing the influence of the vacuum-pipe on the radiation pulse as a function of the problem parameters. Our theory, that makes consistent use of dimensionless analysis, allows treatment and physical understanding of many asymptotes of the parameter space, together with their region of applicability. **A more detailed report of our study is given in [1]**.

INTRODUCTION AND THEORY

The accelerator complex at FLASH produces ultrashort bunches approaching sub-100 fs duration. FLASH will soon operate together with a FIR electromagnetic undulator providing coherent FIR radiation intrinsically synchronized with the VUV pulses. The wavelength range ($\lambda = 60 \div 200$ μm) will overlap with a large part of the THz-gap. This will allow pump-probe experiments combining FIR and VUV radiation, and non-destructive electron beam diagnostics. Vacuum chamber effects are expected to play an important role at longer wavelengths. Optimization of the radiation transport system calls for a precise characterization of THz pulses along the photon beamline. In the present work we focus on the characterization of undulator radiation from a filament beam (as for the FIR line at FLASH) in presence of a waveguide. One should solve the field equations in paraxial approximation with proper boundary conditions, e.g. $\mathcal{D}[\vec{\vec{E}}_\perp(z,\vec{r}_\perp)] = \vec{f}(z,\vec{r}_\perp)$, where $(\vec{n}\times\vec{\vec{E}}_\perp)_{|_S} = 0$ and $(\vec{\nabla}_\perp\cdot\vec{\vec{E}}_\perp)_{|_S} = 0$. Here S is the internal surface of the pipe, $\mathcal{D} \equiv (\nabla_\perp{}^2 + 2i\omega/c\cdot\partial/\partial z)$, $\nabla_\perp{}^2$ being the Laplacian operator over transverse cartesian coordinates and $\vec{f} = 4\pi e/c\cdot\exp\{i\int_0^z d\bar{z}\omega/[2\gamma_z^2(\bar{z})c]\}[i\omega/c^2\cdot\vec{v}_\perp(z) - \vec{\nabla}_\perp]\delta(\vec{r}_\perp - \vec{r}'_\perp(z))$. Solution must accounting for the tensorial nature of the Green's function. In the UR case, the resonance approximation can be exploited too. We thus consider planar undulator with a large number of undulator periods and a frequency range of interest close to the fundamental harmonic, where the free-space field exhibits horizontal polarization (for undulator field in the vertical direction) and azimuthal symmetry. An explicit expression for the field is calculated as a superposition of TE and TM modes. We introduce normalized units: $\hat{\vec{\vec{E}}}_\perp = [-c^2/(A_{JJ}\omega e\theta_s)]\vec{\vec{E}}_\perp$, $\hat{C} = 2\pi N_w\Delta\omega/\omega_r$, $\hat{z} = z/L_w$, $\hat{r} = r/\sqrt{L_w\lambda\!\!\!^{-}}$, $\Omega = R^2/L_w\lambda\!\!\!^{-}$, $\hat{C}_k^\mu\mu_{1k}^2/(2\Omega)$ and $\hat{C}_k^\nu = \nu_{1k}^2/(2\Omega)$. Here $\Omega = R^2/(\lambda\!\!\!^{-}L_w)$ is the main parameter of our theory, comparing the pipe area with the radiation diffraction area, while μ_{mk} and ν_{mk} are, respectively, solutions of $J'_m(\mu_{mk}) = 0$ and $J_m(\nu_{mk}) = 0$. We obtain for $\hat{E}_{x,y}(\hat{r},\phi,\hat{z})$:

$$\hat{E}_x = i\sum_{k=1}^{\infty}\left\{\mathcal{A}_k^\mu(\hat{z})\left[J_o\left(\frac{\mu_{1k}\hat{r}}{\sqrt{\Omega}}\right) + J_2\left(\frac{\mu_{1k}\hat{r}}{\sqrt{\Omega}}\right)\cos(2\phi)\right] + \mathcal{A}_k^\nu(\hat{z})\left[J_o\left(\frac{\nu_{1k}\hat{r}}{\sqrt{\Omega}}\right) - J_2\left(\frac{\nu_{1k}\hat{r}}{\sqrt{\Omega}}\right)\cos(2\phi)\right]\right\} \quad (1)$$

and

$$\hat{E}_y = i\sum_{k=1}^{\infty}\left\{\mathcal{A}_k^\mu(\hat{z})J_2\left(\frac{\mu_{1k}\hat{r}}{\sqrt{\Omega}}\right) - \mathcal{A}_k^\nu(\hat{z})J_2\left(\frac{\nu_{1k}\hat{r}}{\sqrt{\Omega}}\right)\right\}\sin(2\phi), \quad (2)$$

where we set $\mathcal{A}_k^\mu(\hat{z}) = \hat{C}_k^\mu\exp[-i\hat{C}_k^\mu\hat{z}]/[(\mu_{1k}^2-1)J_1^2(\mu_{1k})]\,\mathrm{sinc}[1/2(\hat{C}_k^\mu + \hat{C})]$ and, moreover, $\mathcal{A}_k^\nu(\hat{z}) = \hat{C}_k^\nu\exp[-i\hat{C}_k^\nu\hat{z}]/[\nu_{1k}^2J_0^2(\nu_{1k})]\mathrm{sinc}[1/2(\hat{C}_k^\nu + \hat{C})]$. The sinc(·) functions in the expressions for $\mathcal{A}_k^{\mu,\nu}$ is consequence of instantaneous switching of the undulator field. However, our theory applies with a finite accuracy related to the use of the resonance approximation. We thus introduce a spatial frequency filter in the field by redefining

$$\mathcal{A}_k^\mu(\hat{z}) = \frac{\hat{C}_k^\mu\exp[-i\hat{C}_k^\mu\hat{z}]}{(\mu_{1k}^2-1)J_1^2(\mu_{1k})}\mathcal{F}\left\{S(\hat{z}'),\left(\hat{C}_k^\mu + \hat{C}\right)\right\} \quad (3)$$

and

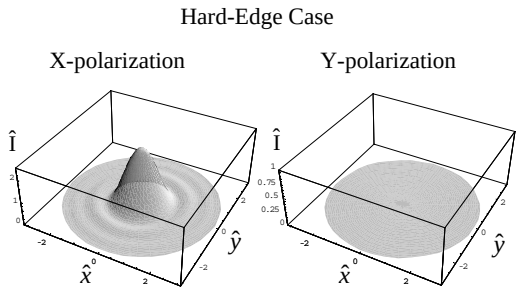

Figure 1: Three-dimensional view of the virtual source in the free-space limit for $\Delta = 0$ (hard-edge case) and $\hat{C} = 0$ (perfect resonance) .

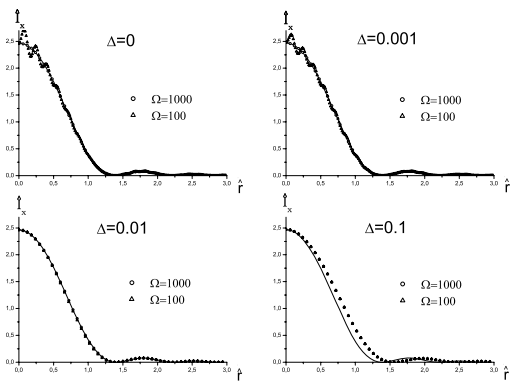

Figure 2: Intensity profiles of the virtual source ($\hat{z} = 0$) at large values of $\Omega = R^2/(\lambda L_w)$ for different values of Δ and $\hat{C} = 0$ (perfect resonance). This 2D plot is obtained cutting the 3D intensity profile at $\hat{y} = 0$ (i.e. at $\phi = 0$).

$$\mathcal{A}_k^{\nu}(\hat{z}) = \frac{\hat{C}_k^{\nu}\exp[-i\hat{C}_k^{\nu}\hat{z}]}{\nu_{1k}^2 J_0^2(\nu_{1k})}\mathcal{F}\left\{S(\hat{z}'),\left(\hat{C}_k^{\nu}+\hat{C}\right)\right\} . \qquad (4)$$

Here $\mathcal{F}\{S(\hat{z}'),(\hat{C}_k^{\mu,\nu}+\hat{C})\}$ is the Fourier transform of the function S with respect to $(\hat{C}_k^{\mu,\nu}+\hat{C})$. The where function $S(z')$ introduces some smoothing of the rectangular undulator profile on a scale of λ_w. We model $S(\hat{z}')$ as a constant function along the undulator length with exponentially decaying edges on a typical distance Δ. The value of Δ is chosen to cut off high spatial frequencies that are outside the region of applicability of the resonance approximation, i.e. $\Delta \sim 1/N_w$. A three-dimensional view of the virtual source in the middle of the undulator in the free-space limit $\Delta = 0$ (hard-edge case) is presented in Fig. 1, while intensity profiled for different values of Δ are given in Fig. 2.

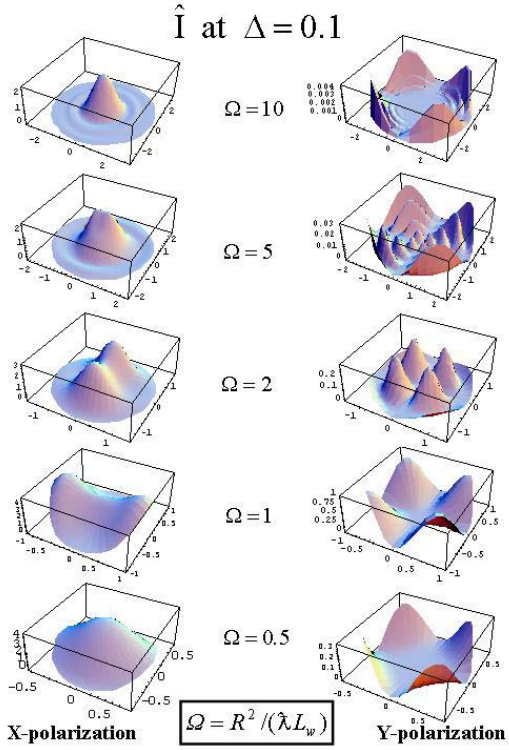

Figure 3: Intensity profiles of the virtual source ($\hat{z} = 0$) at different values of $\Omega = R^2/(\lambda L_w)$ for $\Delta = 0.1$ and $\hat{C} = 0$ (perfect resonance).

We also studied the impact of wall-resistance effects. We concluded that propagation through the pipe is strongly affected by wall-resistance effects even for relatively large values of Ω. This effect strongly depends on the material considered. Estimations allowed us to formulate the recommendation that the internal part of the vacuum pipe for the infrared undulator line at FLASH should be copper-coated.

RESULTS

Some figure of merit should be extracted from the full information carried by the expression for the field about how the metallic pipe influences radiation properties. We separately studied, for horizontal and vertical polarization components, two-dimensional intensity distributions on a transverse plane at arbitrary distance from the undulator, for different choices of the problem parameter. These plots are shown in Fig. 3 and Fig. 4. Another figure of merit of interest is the ratio between the power density for a specific value of Ω integrated over the waveguide cross-section and the angle-integrated power density in free space:

$$\hat{W} = \int d\vec{\hat{r}}_{\perp}\left|\vec{\hat{E}}_{\perp}(\Omega)\right|^2 \Big/ \left(\int d\vec{\hat{r}}_{\perp}\left|\lim_{\Omega\to\infty}\vec{\hat{E}}_{\perp}\right|^2\right) . \qquad (5)$$

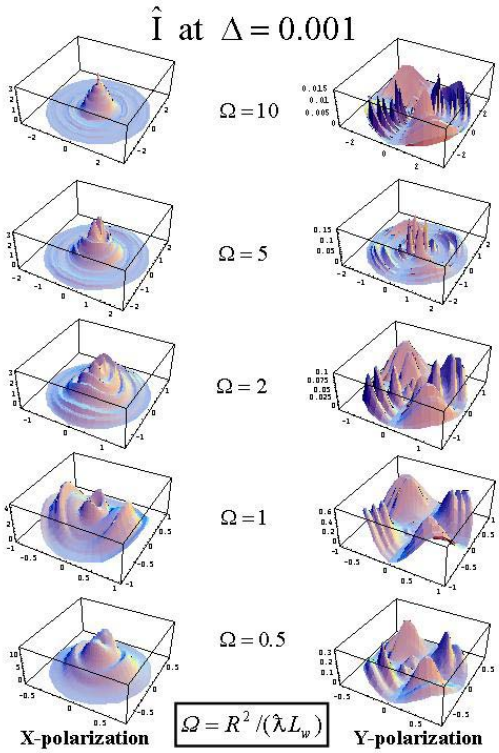

Figure 4: Intensity profiles of the virtual source ($\hat{z} = 0$) at different values of $\Omega = R^2/(\lambda L_w)$ for $\Delta = 0.001$ and $\hat{C} = 0$ (perfect resonance).

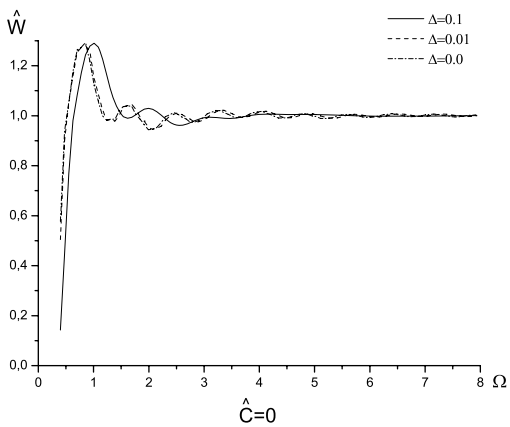

Figure 5: Plot of $\hat{W}$ as a function of $\Omega = R^2/(\lambda L_w)$ for $\hat{C} = 0$ (perfect resonance) at different values of Δ.

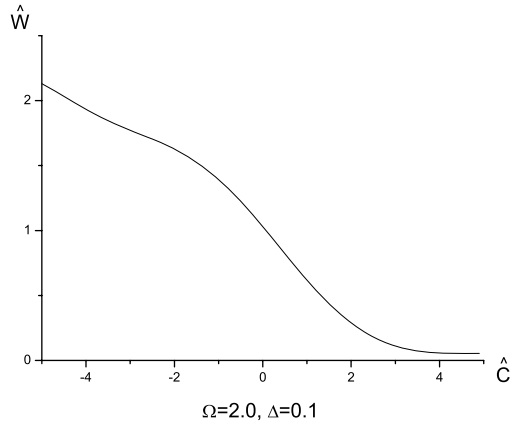

Figure 6: Plot of $\hat{W}$ as a function of $\hat{C} = 2\pi N_w \Delta\omega/\omega_r$ for $\Omega = 2.0$ at $\Delta = 0.1$.

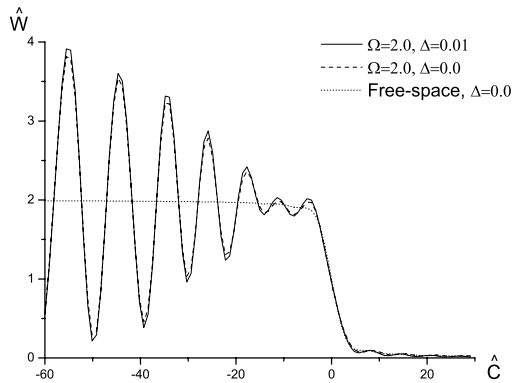

Figure 7: Plot of $\hat{W}$ as a function of $\hat{C} = 2\pi N_w \Delta\omega/\omega_r$ for $\Omega = 2.0$ at different values of $\Delta = 0.01$ and $\Delta = 0$. The far-field limit ($\Omega \longrightarrow \infty$) is also shown for comparison (dotted line).

We studied $\hat{W}$ as a function of Ω at perfect resonance (see Fig. 5). Conversely, once Ω is fixed, one can investigate how the total power changes as a function of the detuning from resonance (see Fig. 6 and 7).

We also proposed a comparison between the magnitude of the horizontally and vertically polarized fields, defined as

$$P_x(\hat{r}) = \mathrm{Abs}\left[\hat{E}_x(\hat{r}, 0, 0)\right]\Big|_{\Omega\longrightarrow\infty} \tag{6}$$

and

$$P_y(\hat{r}, \Omega) = \mathrm{Abs}\left[\hat{E}_y\left(\hat{r}, \frac{\pi}{4}, 0\right)\right]\Big|_{\Omega} . \tag{7}$$

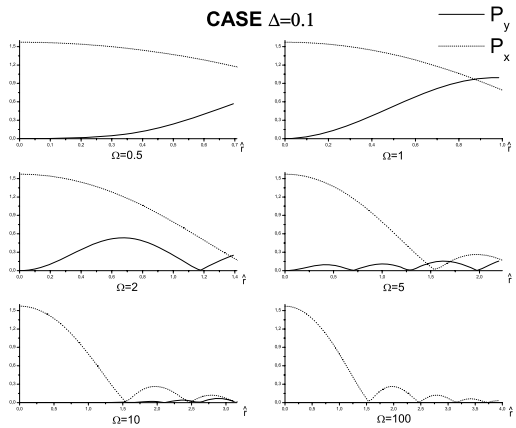

Figure 8: Comparison of P_x (dotted line) and P_y (solid line) for $\Delta = 0.1$ at different values of $\Omega = R^2/(\lambda L_w)$ and $\hat{C} = 0$ (perfect resonance). Plots refer to the virtual source position ($\hat{z} = 0$).

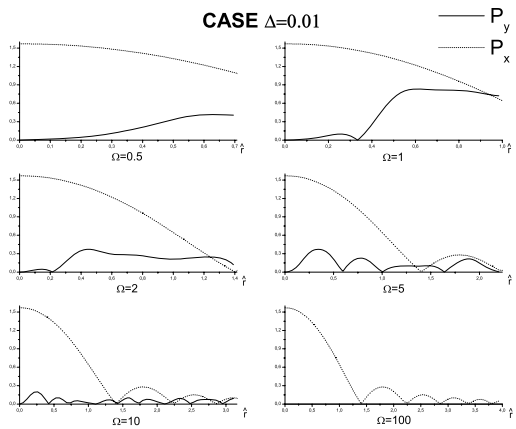

Figure 9: Comparison of P_x (dotted line) and P_y (solid line) for $\Delta = 0.01$ at different values of $\Omega = R^2/(\lambda L_w)$ and $\hat{C} = 0$ (perfect resonance). Plots refer to the virtual source position ($\hat{z} = 0$).

Plots are given in Fig. 8 and Fig. 9.

Finally, evolution of the intensity profiles at $\Omega = 2$ and $\hat{C} = 0$ is given in Fig. 9.

CONCLUSIONS

We presented a theory of undulator radiation within a waveguide and we exemplified it in the case of the infrared undulator beamline at FLASH. Relation between current electromagnetic sources and field is more complicated with respect to the free-space case. Analysis of the problem is performed with the help of

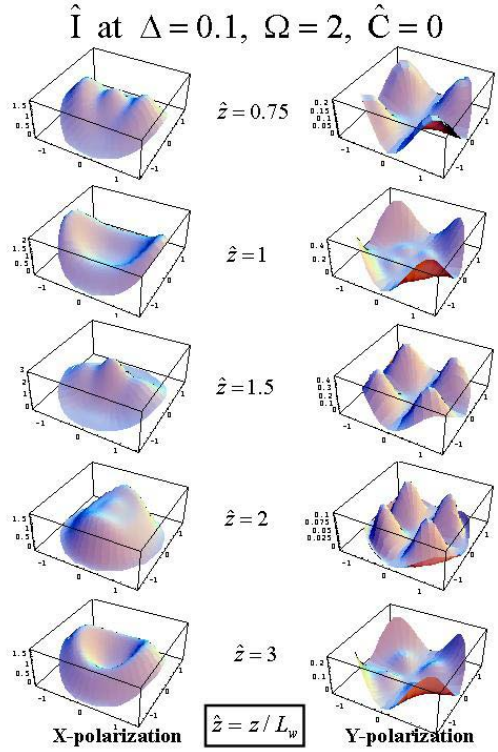

Figure 10: Intensity profiles at different values of $\hat{z} = z/L_w$ for $\Omega = 2$, $\hat{C} = 0$ (perfect resonance) and $\Delta = 0.1$.

a tensor Green's function, complicating equations that now depend on the undulator type and on the waveguide geometry. We treated a circular waveguide in particular, and we implemented the planar undulator case within the applicability region of the resonance approximation. The electric field was found as a superposition of the waveguide modes, and was studied for different values of parameters. The main parameter involved in the problem is the waveguide parameter Ω. When Ω is comparable, or smaller than unity, waveguide effects become important, under the assumption of a perfect conductor.

For details on our work we refer the interested reader to [1].

REFERENCES

[1] G. Geloni, E. Saldin, E. Schneidmiller and M. Yurkov,submitted to Elsevier Science, also DESY 07-31 (2007) http://arxiv.org/abs/physics/0703049.